Journal of Power Sources 189 (2009) 121–126

Contents lists available at ScienceDirect

Journal of Power Sources

journal homepage: www.elsevier.com/locate/jpowsour

# Preparation and characterization of a new nanosized silicon–nickel–graphite composite as anode material for lithium ion batteries

Xiuyan Wang, Zhaoyin Wen*, Yu Liu, Xiaogang Xu, Jiu Lin

*Shanghai Institute of Ceramics, Chinese Academy of Sciences, 1295 Dingxi Road, Shanghai 200050, PR China*

ARTICLE INFO

*Article history:*
Received 28 June 2008
Received in revised form 8 October 2008
Accepted 10 October 2008
Available online 21 October 2008

*Keywords:*
Silicon–nickel–graphite
Lithium ion battery
Anode
Composite
HEMM

ABSTRACT

A new type of nanosized silicon–nickel–graphite (Si–Ni–G) composite was prepared by high energy mechanical milling (HEMM) and pyrolysis using SiO as the precursor of Si for the first time. X-ray diffraction (XRD), high-resolution transmission electron microscope (HRTEM) and scanning electron microscopy (SEM) were used to determine the phases obtained and to observe the microstructure and distribution of the composite. The composite powders consisted of Si, Ni, $SiO_2$, NiO and a series of Si–Ni alloys. The formation of the inactive $SiO_2$ and Si–Ni alloy phases could accommodate the large volume changes of the active particles during cycling. In addition, cyclic voltammetry (CV) and galvanostatic discharge/charge tests were carried out to characterize the electrochemical properties of the composite. The composite electrodes exhibited an initial discharge and charge capacity of 1450.3 and 956.4 mAh $g^{-1}$, respectively, maintaining a reversible capacity of above 900 mAh $g^{-1}$ for nearly 60 cycles.



## 1. Introduction

Currently, with the development of portable devices and electric vehicles, lithium ion-batteries with high energy density and long cycle life have been given high demand. However, the development of lithium ion-batteries is limited due to the low theoretical capacity (372 mAh $g^{-1}$) of the commercialized carbon anode materials [1,2]. Therefore, great efforts to find alternative anode materials are underway. Silicon is of special interest because of its potentially large theoretical specific capacity (up to 4.2 mole of Li per mole Si) as well as its satisfactory potential for lithium insertion and extraction (<0.5 V vs. $Li/Li^+$) [3]. One of the critical problems encountered with this anode is the severe volume change during the alloying and dealloying reaction with lithium ions. The volume change of $Li_{4.2}Si$ is approximately four times that of Si, according to the estimates based on lattice parameters of their crystal structures. It is considered that the expansion and contraction during the charge–discharge cycling leads to the pulverizing of the silicon particles. This would cause the breakdown of the electrode, resulting in the loss of capacity within several cycles [4–6].

As an alternative, SiO appears particularly promising because of its long cycle life [17]. It also has the advantage of absorbing and retaining a large quantity of lithium, which gives it a higher specific capacity (2043 mAh $g^{-1}$) than lithium–graphite [7,8]. Recently, $SiO_x$-based composites as anode materials for lithium ion batteries have been given much report [9–11]. Moritaz et al. [9] reported a nano Si cluster-$SiO_x$–C composite as anode materials for lithium ion batteries prepared by ball-milling and heat treatment under high temperature, which showed higher capacity and enhanced cycle life, but the irreversible capacity at initial cycles needed to be reduced. Kim et al. [10] synthesized a SiO–C composite by ball-milling followed by pyrolyzing with polyvinyl alcohol (PVA). The composite displayed improved initial cycling efficiency and higher reversible capacity than those of the commercial graphite anodes. However, the inactive SiC was formed during the pyrolysis. Yuan et al. [11] synthesized a CX (Carbon xerogel)–SiO composite by high energy mechanical milling of the CX prepared by themselves and commercial SiO which could get better cycling performance than that of the CX, but the initial columbic efficiency was only 47.8%.

In our work, we prepared a new nanosized silicon–nickel–graphite composite by high energy mechanical milling (HEMM) followed by pyrolysis at 800 °C for 5 h. SiO was chosen as the source of Si. Nickel powder and graphite were added during the milling process in order to get a composite with improved cycling performance and good conductivity. During the preparation, SiO was transformed into Si and $SiO_2$. The $SiO_2$ would act as a matrix which was capable of bonding firmly to Si and fixing them during charge–discharge cycles [9]. A series of Si–Ni alloy phases and a contamination of $Al_2O_3$ also appeared in the XRD patterns, which could buffer the volume changes [14–16]. The composite electrodes revealed a reversible capacity of more than 900 mAh $g^{-1}$ for nearly 60 cycles.

* Corresponding author. Tel.: +86 21 52411704; fax: +86 21 52413903.
*E-mail address:* zywen@mail.sic.ac.cn (Z. Wen).

0378-7753/$ – see front matter © 2008 Elsevier B.V. All rights reserved.
doi:10.1016/j.jpowsour.2008.10.041

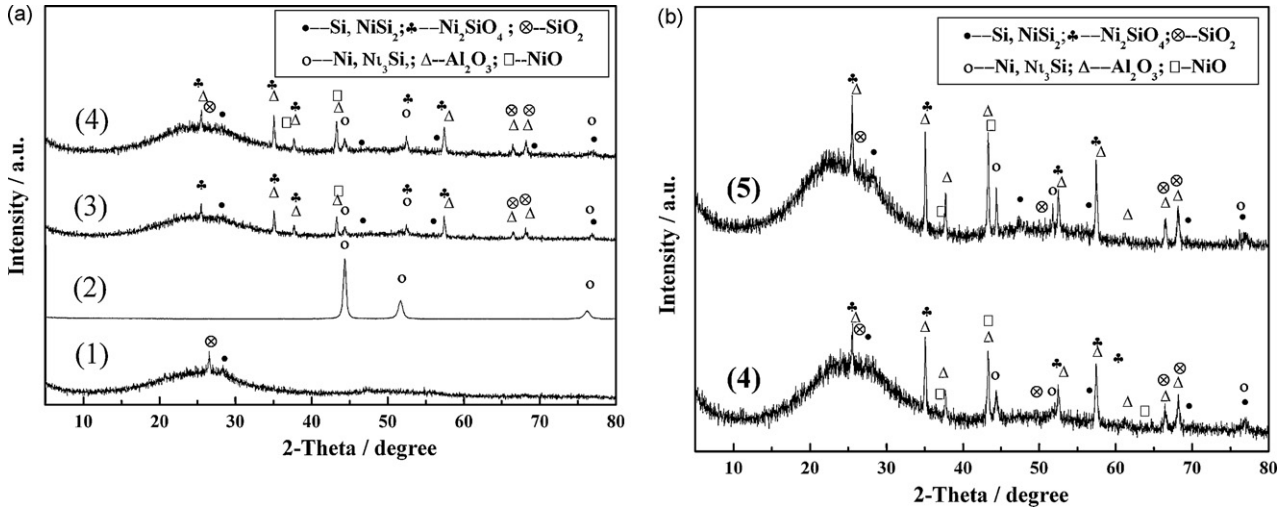


**Fig. 1.** X-ray diffraction patterns of (1) SiO milled for 5 h; (2) nickel powder milled for 5 h; (3) (SiO + Ni) milled for 3.5 h; (4) sample 3 + 15 wt.% of graphite milled for 1.5 h and (5) sample 4 heated at 800 °C under vacuum for 5 h.

## 2. Experimental

The starting materials of silicon monoxide (SiO, 99.99%, Shanghai Chemical Co. Ltd., China) and nickel powder (0.8 wt.%, Shanghai Chemical Co. Ltd., China) were transferred into an 80 ml alumina vial in an argon-filled glove box (Korea Kiyon) for mechanical milling. The ball-milling was carried out in a Planetary Mono Mill P-5 (Fritsch, Germany) at a rotation rate of 350 (766.5) rpm. The

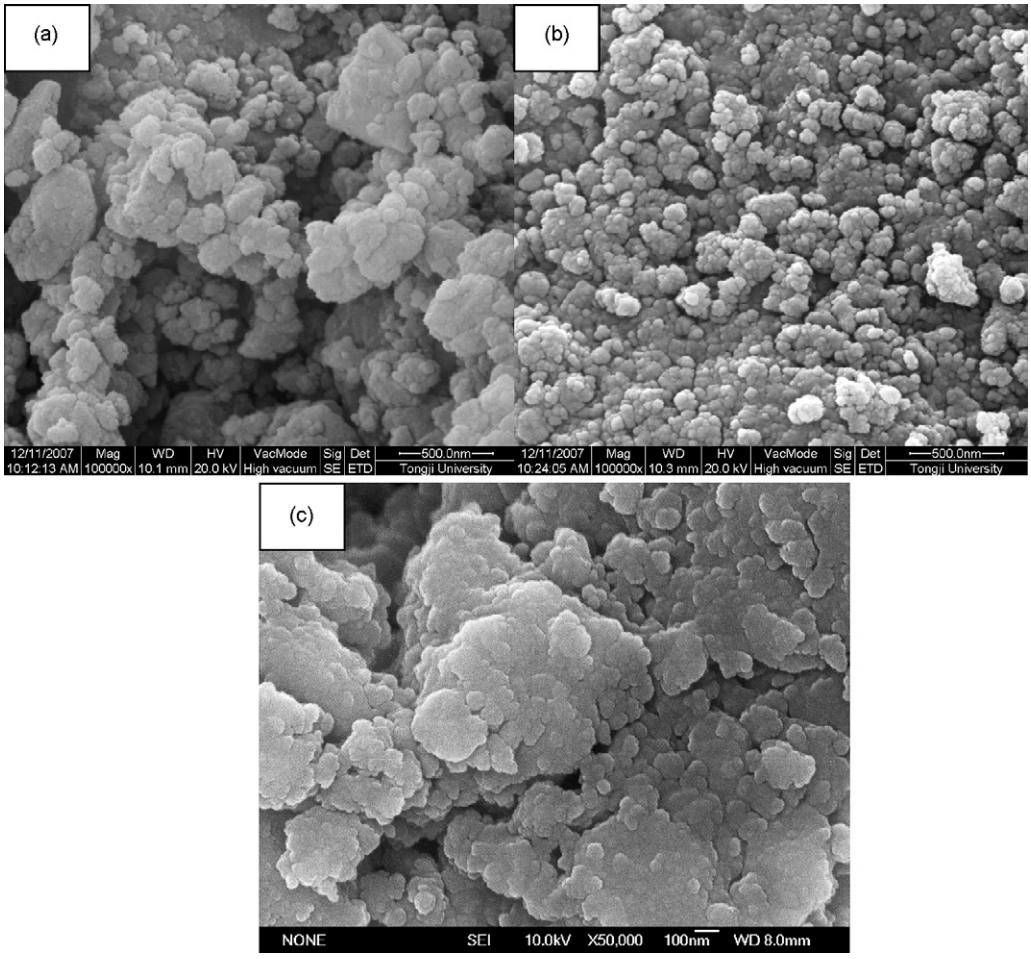


**Fig. 2.** SEM morphology of: (a) (SiO + Ni) milled for 3.5 h; (b) the sample (a) +15 wt.% of graphite milled for 1.5 h; (c) the sample (b) heated at 800 °C under vacuum for 5 h.

mass ratio of the milling balls and the reactants was 10:1. After 3.5 h of milling, 15 wt.% of graphite was added into the vial as a dispersion agent and further milled for 1.5 h. The as-milled powder was heated at 800 °C under vacuum for 5 h, and the final product was obtained without any grinding and sieving. In addition, pure SiO and Si powder milled for 5 h were prepared to make a comparison.

The sample was characterized by X-ray diffraction (XRD, Rigaku RINT-2000) with Cu Kα radiation to identify the phases formed. Environmental scanning electron microscope (ESEM Quanata 200 FEG), field emission scanning electron microscope (FESEM JSM-6700F) and transmission electron microscope (TEM, JEM-2010) were applied to observe the morphology and particle size of the synthesized composite materials.

Electrodes containing 60 wt.% active materials (the as-prepared composite), 20 wt.% polyvinylidene fluoride (PVDF) binder and 20 wt.% carbon black were made by coating the slurry of the electrode ingredients in *N*-methyl pyrrolidinone (NMP) onto copper foil and dried at 100 °C under vacuum for 10 h. The thickness of the electrodes was about 28 μm. The working electrodes were assembled in 2025 coin cells using Celgard 2400 as the separator and lithium foils as the counter and reference electrodes. A solution of 1 M $LiPF_6$ in EC:DMC (1:1 weight) was employed as the electrolyte. The assembly of cells was processed in an argon filled glove box with oxygen and water contents less than 1 ppm. The galvanostatic charge/discharge tests were conducted on a LAND CT2001A battery test system in a voltage range of 0.02–1.5 V (vs. $Li/Li^+$) at a current density of 0.1 mA $cm^{-2}$. The cyclic voltammetry experiments were performed on a CHI760C Electrochemical Workstation.

## 3. Results and discussion

### 3.1. Phase analysis

Fig. 1 showed the X-ray diffraction patterns of the composite during different preparation steps as well as the SiO and Ni powder. As seen from curve 3 in Fig. 1(a), when SiO and Ni were milled for 3.5 h, the peaks of elemental Si, $SiO_2$, NiO, $Ni_2SiO_4$ as well as Ni–Si alloys were observed, implying the decomposition of SiO assumed as reaction (1) during the HEMM process. Since the appearance of NiO and $Ni_2SiO_4$, reactions (2) and (3) might also occur. The reactions were summarized as follows:

$$2SiO = Si + SiO_2 \quad (1)$$

$$SiO + Ni = Si + NiO \quad (2)$$

$$SiO_2 + 2NiO = Ni_2SiO_4 \quad (3)$$

As a contamination, $Al_2O_3$ (about 0.6 wt.% of elemental Al in the composite) was also observed which might act as an effective matrix [16]. When 15 wt.% of graphite was added and further milled for 1.5 h, as shown in curve 4, the composite displayed the same diffraction patterns as curve 3. When the as-milled powder was heated at 800 °C under vacuum for 5 h, no any further change of the XRD pattern was observed (curve 5), while the intensity of the peaks was reinforced. There was no SiC phase was observed in the

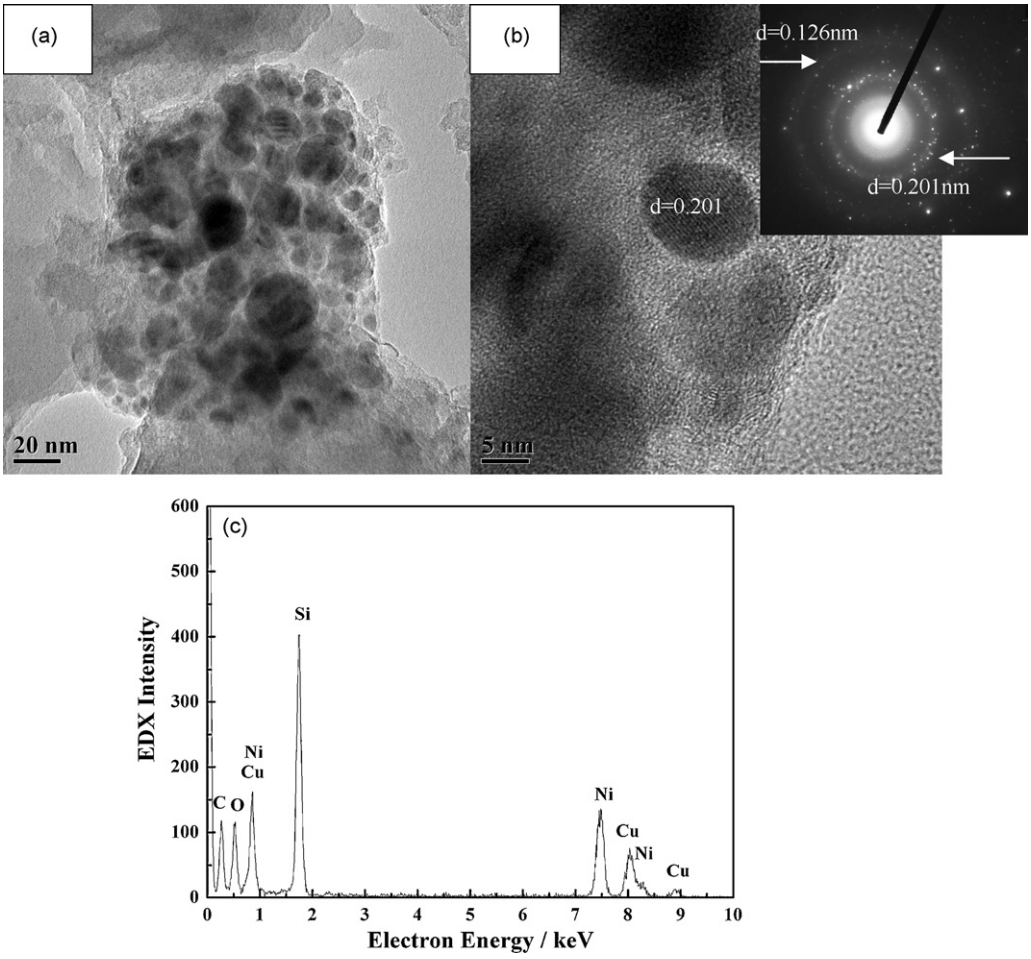


**Fig. 3.** (a) The TEM image of the composite powder, (b) the HRTEM image and the SAED image of the composite powder, and (c) the XEDS pattern of the black particle in (a).

XRD pattern after heat-treatment. The intensity increase implied further growth of the particle under heat-treatment.

### 3.2. Morphological feature

The morphology of the milled powders was observed by SEM. Fig. 2(a) showed the secondary electron image of the SiO and Ni milled for 3.5 h. It was seen that the composite powder consisted of clusters with size of dozens of hundreds of nanometers. The Ni metal was ductile and it could be easily agglomerated with Si during the HEMM process. When 15 wt.% of graphite was added and further milled for 1.5 h, as shown in Fig. 2(b), the agglomeration of the particles was alleviated and the particle size was more uniform, which could be attributed to the dispersion and lubrication of the graphite. Fig. 2(c) showed the morphology of the as-milled composite heated at 800 °C under vacuum for 5 h. As could be seen, the morphology of the agglomerates became flat while in Fig. 2(b) it was global. The difference might be due to the decomposition of the residual SiO and the further formation of Si–Ni alloys, which would result in the recombination of the particles.

In order to observe the primary particles of the composite and to further confirm its phases, the transmission electron microscope (TEM) with X-ray energy-dispersive spectrometry (XEDS) and high-resolution transmission electron microscope (HRTEM) with selected area electron diffraction (SAED) were used and the results were shown in Fig. 3. In the TEM image (Fig. 3(a)), black dots with size of 10–20 nm distributed uniformly were observed. In the HRTEM image (Fig. 3(b)), the lattice fringe was observed on some of the black dots. The interplanar distance (*d*-spacing) as shown in the inset of Fig. 3(b) agreed with Ni (1 1 1), Ni (2 2 0) and $Ni_3Si$ ($\bar{2}$ 2 0), $Ni_3Si$ ($\bar{3}$ 1 4), which were well coincident with the XRD patterns. Fig. 3(c) showed the XEDS image of the black area in Fig. 3(a) in the range of 100 nm. It was clear that the black particles mainly consisted of Si and Ni and a little amount of C and O. However, the lattice fringe of Si was not observed, which might be due to its amorphous structure.

### 3.3. Cyclic voltammograms

The cyclic voltammograms of the as-prepared composite electrodes in the potential window from 0 to 1.5 V (vs. $Li^+/Li$) at different scan rates were shown in Fig. 4. Fig. 4(a) showed the comparison among the 1st the cyclic voltammogram of the as-prepared composite electrode, the SiO electrode and the Si electrode at the scan rate of 0.05 mV $s^{-1}$. As seen, the cyclic voltammogram of the composite electrode was different from those of Si and SiO electrodes. During the first reduction scanning process, the composite electrode experienced a weak and broad peak in the range of 0.6–0.9 V (the circled area) corresponding to the formation of a solid electrolyte interface (SEI) film on the surface of active particles [12],

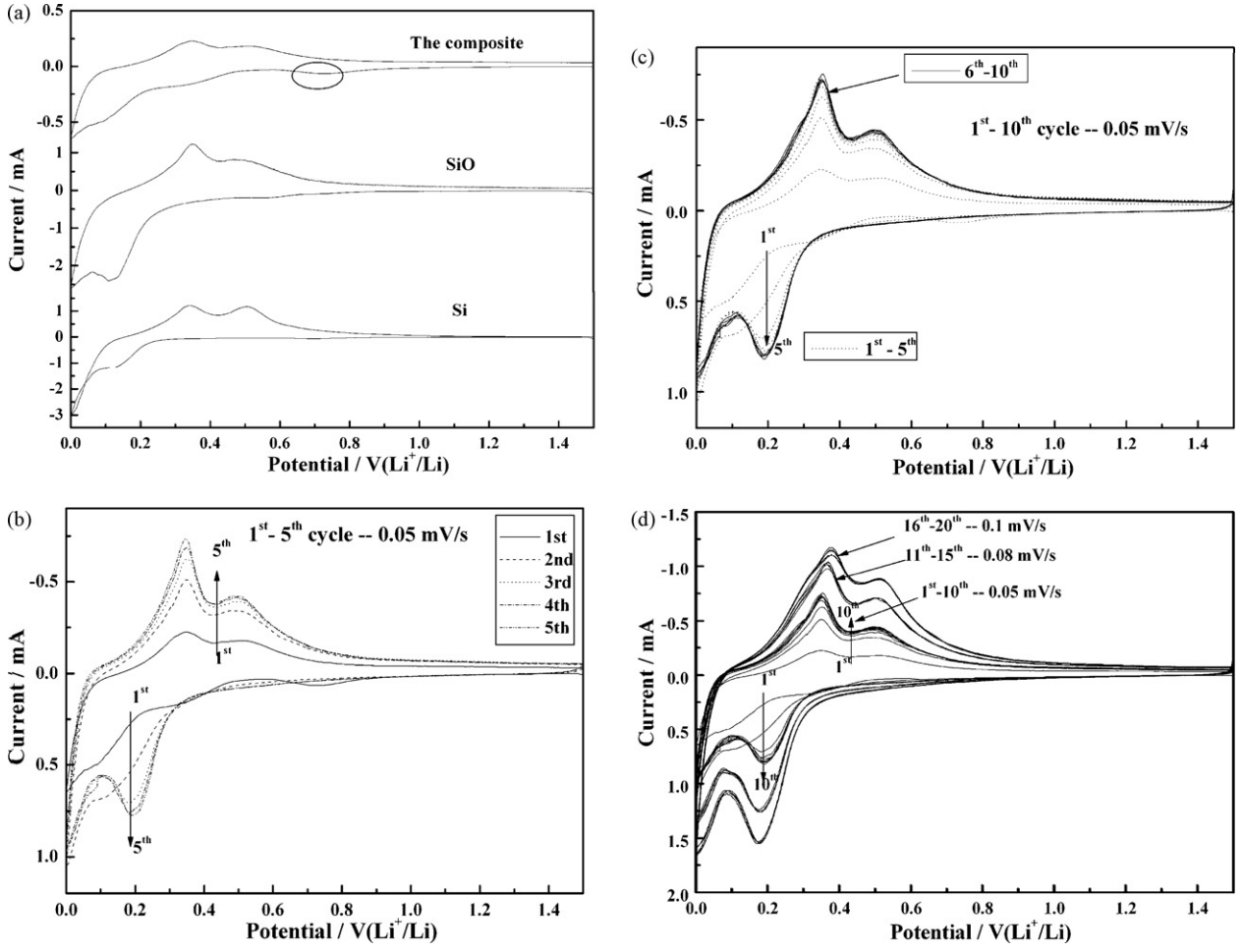


**Fig. 4.** Cyclic voltammograms in the potential window from 0 to 1.5 V (vs. $Li^+/Li$) of (a) the comparison of the 1st cycle among the as-prepared composite electrode, the SiO electrode and the Si electrode at the scan rate of 0.05 mV $s^{-1}$; (b) the 1st to 5th cycles of the as-prepared composite electrode at 0.05 mV $s^{-1}$; (c) the 1st to 10th cycles at 0.05 mV $s^{-1}$; and (d) the comparison among the 1st to 10th cycles at 0.05 at mV $s^{-1}$, 11th to 15th cycles at 0.08 mV $s^{-1}$ and 16th to 20th cycles at 0.1 mV $s^{-1}$.

and a weak peak in the range of 0.45–0.25 V corresponding to the formation of $Li_{12}Si_7$ [3]. The sharp reduction peak from 0.2 to 0 V also appeared corresponding to the formation of lithium-rich $Li_xSi$ phases [3]. While for the pure Si electrode there was only one sharp reduction peak from 0.2 to 0 V, and for the pure SiO electrode there were two sharp reduction peaks at about 0.1 and 0 V. The capacity loss resulted from the formation of SEI could be negligible in the pure Si and SiO electrode, which might be due to the existence of silicon oxide on the surface that hindered the decomposition of the electrolyte [13]. There was no obvious difference among the composite, the pure Si and SiO electrodes in the 1st oxidation scanning process. The cyclic voltammogram of the as-prepared composite electrode was more like that of the pure Si electrode.

In the subsequent cycles as shown in Fig. 3(b), the oxidation peaks were almost the same as the first scan, while the reduction peaks were different. A new reduction peak occurred at about 0.2 V which could also be corresponding to the lithium insertion process of elemental silicon. In addition, from the 1st to 5th cycles, the current of the redox reactions increased with cycling, implying a possible activation process during the insertion/extraction process [8,18]. While in the subsequent 6th to 10th cycles (shown in Fig. 3(c)), the redox peaks were overlapped together. When the scanning rate increased to 0.08 and 1.0 mV $s^{-1}$ (Fig. 3(d)), the positions of the redox peaks were almost the same as those occurred at 0.05 mV $s^{-1}$, which demonstrated that the microstructure of the composite electrode became steady after the initial cycles.

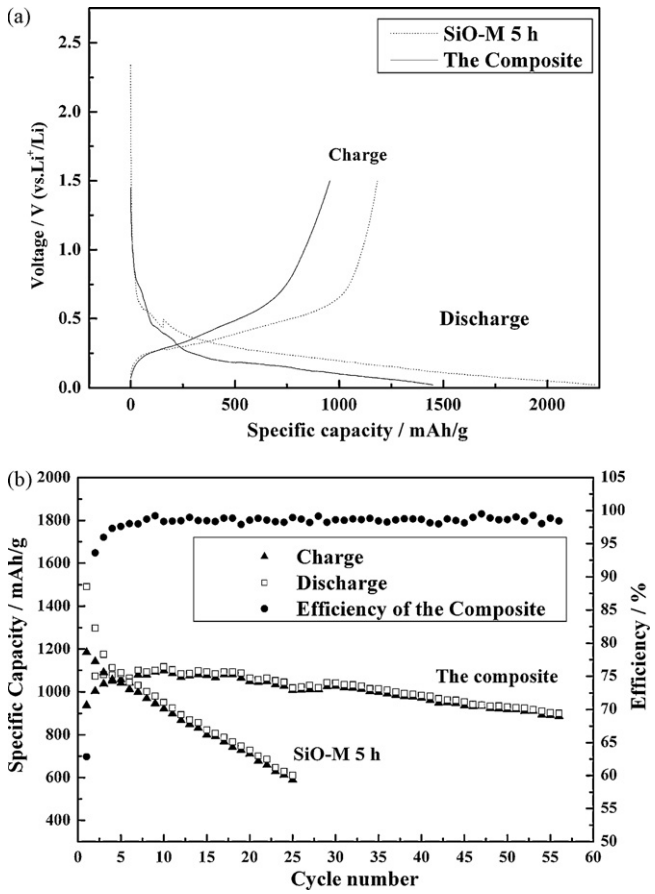


**Fig. 5.** (a) The discharge and charge curves for the as-prepared composite electrode and the pure SiO electrode at 0.1 mA $cm^{-2}$. (b) The cycling performances of the as-prepared composite electrode and the pure SiO electrode.

### 3.4. Cycling performance

Fig. 5(a) showed the discharge and charge curves of the as-prepared composite electrode and the pure SiO electrode in the voltage range of 0.02–1.5 V (vs. $Li^+/Li$) at the current density of 0.1 mA $cm^{-2}$. The first cycle began with discharging process, corresponding to the lithium insertion of the electrodes. From the figure, we could see that there was a little difference on the discharge platforms between the composite electrode and the SiO electrode, which were coincident with the cyclic voltammograms. For the SiO electrode, the first discharge and charge capacity were 2228.7 and 1183.5 mAh $g^{-1}$ respectively, with a columbic efficiency of only 53%. For the composite electrode, the first discharge and charge capacity were 1450.3 and 956.4 mAh $g^{-1}$ respectively, and the columbic efficiency was about 66% which was much higher than that of the SiO electrode.

Fig. 5(b) showed the cycling performance of the as-prepared composite electrode and the pure SiO electrode. It was obvious that the cycling performance of the as-prepared composite electrode was much better than that of the pure SiO electrode. For the SiO electrode, the cycling performance was very poor. After 25 cycles, the reversible capacity loss was more than 50%. While the composite electrode revealed a rechargeable capacity of above 900 mAh $g^{-1}$ for nearly 60 cycles and the reversible capacity retention was more than 95%. We believed that the reason for the improved cycling performance could be ascribed as follows: (i) the uniform distribution of the active particles in the inactive matrix and the reduced particle size by HEMM which increased the mechanical stability [8,10]; (ii) the formation of $SiO_2$ and the inactive Si–Ni alloy phases, as well as the existence of the graphite which could act as dispersing agents and buffering matrixes and could maintain the integrality of the electrodes with cycling [8–10]; and (iii) the introduction of Ni and graphite which could provide better electric contact during cycling.

## 4. Conclusions

A new type of nanosized silicon–nickel–graphite (Si–Ni–G) composite was prepared using SiO as the precursor of Si by high energy mechanical milling and pyrolysis for the first time. The composite powders consisted of Si, Ni, $SiO_2$, NiO, $Ni_2SiO_4$ and a series of Si–Ni alloys. The formation of the inactive $SiO_2$ and Si–Ni alloy phases could accommodate the large volume changes during cycling. The introduction of Ni and graphite could provide better electrical contact during cycling. The composite electrodes revealed a rechargeable capacity of above 900 mAh $g^{-1}$ for nearly 60 cycles, with a reversible capacity retention ratio of more than 95%. Although the agglomeration of the composite during the HEMM process and the first efficiency remains to be improved, the Si–Ni–G composite could be a promising candidate as anode material for lithium ion batteries.

## Acknowledgments

This work was financially supported by NSFC Project Nos. 20333040 and 50672114, 863 Project of China No. 2006AA03Z232 and 973 Project of China No. 2007CB209700.

## References

[1] T. Tran, J. Feikert, X. Song, K. Kinoshita, J. Electrochem. Soc. 142 (1995) 3297.
[2] B.A. Johnson, R.E. White, J. Power Sources 70 (1998) 48.
[3] W.J. Weydanz, M. Wohlfahrt-Mehrens, R.A. Huggins, J. Power Sources 81–82 (1999) 237.
[4] L.Y. Beaulieu, K.W. Eberman, R.L. Turner, L.J. Krause, J.R. Dahn, Electrochem. Solid-State Lett. 4 (2001) 137.

[5] Z.P. Guo, J.Z. Wang, H.K. Liu, S.X. Dou, J. Power Sources 146 (2005) 448.
[6] B.C. Kim, H. Uono, T. Satou, T. Fuse, T. Ishihara, M. Ue, J. Electrochem. Soc. 152 (2005) A523.
[7] J. Yang, Y. Takeda, N. Imanishi, C. Capiglia, J.Y. Xie, O. Yamamoto, Solid State Ionics 152–153 (2002) 125.
[8] M. Miyachi, H. Yamamoto, H. Kawai, T. Ohta, M. Shirakata, J. Electrochem. Soc. 152 (10) (2005) A2089.
[9] T. Moritaz, N. Takami, J. Electrochem. Soc. 153 (2) (2006) A425.
[10] J.H. Kim, H.J. Sohn, H. Kim, G. Jeong, W. Choi, J. Power Sources 170 (2007) 456.
[11] X.X. Yuan, Y.J. Chao, Z.F. Ma, X.Y. Deng, Electrochem. Commun. 9 (2007) 2591.
[12] Y. Liu, K. Hanai, J. Yang, N. Imanishi, A. Hirano, Y. Takeda, Electrochem. Solid-State Lett. 7 (2005) A369.
[13] X.D. Wu, Z.X. Wang, L.Q. Chen, X.J. Huang, Electrochem. Commun. 5 (2003) 935.
[14] G.X. Wang, L. Sun, D.H. Bradhurst, S. Zhong, S.X. Dou, H.K. Liu, J. Alloy Compd. 306 (2000) 249.
[15] M.S. Park, Y.J. Lee, Y.S. Han, J.Y. Lee, Mater. Lett. 60 (2006) 3079.
[16] Y. Zheng, J. Yang, Y.N. NuLi, J.L. Wang, J. Power Sources 174 (2007) 624.
[17] H. Yamamoto, M. Miyachi, H. S Kawai, Abstracts of the Electrochemical Society of Japan 2004 Spring Meeting, Yokohama, 2004, p. 204.
[18] Handbook of Philosophy of Electrochemical Measurements, Chemical Industry Press, Beijing, 2006.